

A weighted fuzzy aggregation GIS model in the integration of geophysical data with geochemical and geological data for Pb–Zn exploration in Takab area, NW Iran

M. Farzamian¹ · A. Kamkar Rouhani² · A. Yarmohammadi³ · H. Shahi⁴ ·
H. A. Faraji Sabokbar⁵ · M. Ziaie²

Received: 1 June 2015 / Accepted: 7 October 2015 / Published online: 22 February 2016
© Saudi Society for Geosciences 2016

Abstract Detailed geophysical and geochemical surveys were carried out to determine Pb–Zn mineralization zones in Chichakloo area, east of Takab, Iran. Resistivity and induced polarization (IP) surveys were conducted along 10 parallel profiles on the dolomite unit, and also 292 samples were collected for litho-geochemical studies to assess the extents of Pb–Zn ore deposits in the study area. All exploration data were processed and modeled, and then the results were taken to a geographic information system (GIS) environment to generate a mineral potential map of the area to suggest more accurate or less risky exploration drilling targets. A fuzzy logic approach was used in this study to integrate exploration predictor maps. A new approach was used for fuzzification of the geochemical maps based on the geochemical mineralization probability index (GMPI) calculation, and an approach was proposed to infer a geophysical predictor map from three-dimensional (3D) IP and resistivity maps. Furthermore, the weighted Yager t-norm fuzzy operator was applied for the integration of exploration predictor maps to consider the importance of each map in the mineral potential map generation. The mineral potential map indicates a remarkable overlapping of geophysical and geochemical anomalies in the south of the study area

with a north–south trend. The results of drilling boreholes in the area confirm the obtained mineral exploration results.

Keywords Pb–Zn mineralization · Resistivity · IP · Geochemical surveys · GIS · Fuzzy logic

Introduction

Physical and chemical properties of ore deposits are usually complicated and the necessity of using different exploration methods is unavoidable for mineral exploration. Therefore, an exact interpretation of the results obtained using different exploration methods and quantitative integration of exploration data play important roles in mineral potential mapping. A geographic information system (GIS) as a powerful tool is widely used in regional- and local-scale potential mapping to integrate exploration data such as remote sensing and geological, geophysical, and geochemical maps. Two general GIS modeling approaches are used for mineral potential mapping (Bonham-Carter 1994; Porwal and Kreuzer 2010); the first method consists of data-driven methods. In this approach, the model parameters are determined on the basis of available evidences and the pattern of known mineral deposit(s) in the study area. The methods like weight of evidence (Bonham-Carter et al. 1988; Agterberg 1992; 2011; Tangestani and Moore 2001; Carranza 2004; Ford and Blenkinsop 2008; Fallon et al. 2010), logistic regression (Sinclair and Woodsworth 1970; McCammon 1973; Chung and Agterberg 1980; Harris et al. 2001, 2006), artificial neural networks (Brown et al. 2000; Singer and Kouda 1996, 1997; Porwal et al. 2003a; Harris et al. 2003; Fung et al. 2005; Nykanen 2008), evidential belief functions (Carranza et al. 2005; 2008), and Bayesian classifiers (Porwal et al. 2006) are among the data-driven methods.

✉ M. Farzamian
mohammadfarzamian@fc.ul.pt

¹ Centro de Geofísica, Universidade de Lisboa, Campo Grande Ed. C8, 1749-016 Lisbon, Portugal

² Faculty of Mining and Geophysics, Shahrood University of Technology, Shahrood, Iran

³ Tarbiat Modares University, Tehran, Iran

⁴ Department of Mining Engineering, University of Gonabad, Gonabad, Iran

⁵ Faculty of Geography, Tehran University, Tehran, Iran

Insufficient known mineral occurrences or training sites preclude the use of data-driven methods. However, the knowledge-driven methods or conceptual approach can be used in which the model parameters are specified by an expert opinion considering the exploration target, the area under investigation, and other effective factors in the exploration of mineral deposit(s) (Bonham-Carter 1994; Porwal and Kreuzer 2010). In the knowledge-driven approach, the geoscientist identifies those criteria in the mineral deposit model that are critical to the formation of a mineral deposit. Examples of the knowledge-driven methods include Boolean logic (Bonham-Carter 1994), index overlay (Bonham-Carter 1994), the Dempster–Shafer belief theory (Moon 1990; 1993; An et al. 1994a, 1994b), fuzzy logic (An et al. 1991), and wildcat mapping (Carranza and Hale 2002; Carranza 2010).

Among the knowledge-driven methods, the fuzzy set theory (Zadeh 1965) is extensively used in mineral potential mapping. One of the first applications of fuzzy logic to mineral prospective modeling was described by An et al. (1991). They have applied fuzzy systems for prospecting base metal and iron deposits. The fuzzy logic was then used for prospecting volcanogenic massive sulfide deposits by Eddy et al. (1995), epithermal gold deposits by Carranza et al. (1999), and porphyry copper deposits by Tangestani and Moore (2003). Hybrid fuzzy methods such as neuro-fuzzy modeling (Porwal et al. 2004) and fuzzy weights-of-evidence modeling (Cheng and Agterberg 1999) have been also proposed to optimize utilization of both conceptual knowledge of mineral systems and empirical spatial associations between mineral deposits and evidential features in geocomputational modeling of exploration targets (Carranza 2011). The fuzzy logic approach still remains one of the most widely used mineral prospective models (e.g., Joly et al. 2012; Lusty et al. 2012; Ford and Hart 2013; Yousefi et al. 2013, 2014; Porwal et al. 2014; Yousefi and Carranza 2015).

The main aim of our study is the integration of resistivity, induced polarization (IP), and geochemical and geological data to assess the extents of Pb–Zn ore deposits in Chichakloo area and select the optimal exploration drilling points. To achieve the aim of the study, we first inverted resistivity and IP data to image resistivity and chargeability of the structure in three dimensions. We then converted three-dimensional (3D) resistivity and chargeability images to two-dimensional (2D) maps using the fuzzy logic approach. This approach allows integrating 3D geophysical data with other sources of 2D exploration data. In addition, we processed geochemical data and plotted the geochemical fuzzy coefficient (GFC) map to generate a geochemical predictor map. Despite the traditional approach that categorizes geochemical maps into some classes using arbitrary intervals, the GFC assigns continuous fuzzy values to continuous-value geochemical maps. As shown in several studies (e.g., Yousefi and Carranza 2014), such approaches aim to avoid the

problem of uncertainty due to simplification and discretization of continuous-value spatial evidence into some proximity classes. Afterward, geochemical, geophysical, and geological predictor maps were integrated using the Yager t-norm operator (Kaymak and Sousa 2003) to generate a mineral potential map. This operator is a weighted fuzzy operator which can take into account the importance of each predictor map in mineral potential mapping.

Mineral exploration investigations and data input

Study area

Chichakloo deposit is located in Takab-Zanjan, Iran, in the geographical coordinates of longitude 48° 38' 47" to 48° 39' 48" and latitude 36° 24' 45" to 36° 25' 26", and is situated 30 km from Takab to the east and 25 km far from the world-class Angouran mine.

Geological investigation

Geologically, the study area is located at the contact of the Sanadaj-Sirjan and Urumiyeh-Dokhtar magmatic arc, two geological subdivisions of the Zagros belt (Fig. 1). The Zagros belt formed as a consequence of Tertiary continental collision between the Afro-Arabian plate and smaller Gondwana-derived microplates, after subduction of the Neotethys Ocean during the Cretaceous (Alavi 1994; Gilg et al. 2005). The basement rocks in the Takab-Zanjan area comprise a series of amphibolites, gneisses, micaschists, serpentinites, and marbles affected by greenschist to amphibolite facies metamorphic conditions (Gilg et al. 2005). A Neoproterozoic–Cambrian age of the basement rocks seems highly probable based on the zircon U/Pb dating of a granitic gneiss from the Maneshan area (Stockli et al. 2004) and fossil reports on the occurrences of Early Cambrian fossils (e.g., *Latouchella* sp., *Bemella* sp., and *Halkiera stenobasis*) in marbles near Amirabad (Hamdi 1995).

The study area is quite similar to Angouran deposit in geological units and host rock. The lithology units of the study area consist of sericit, schist, quartzite, and amphibolite that are covered by 40 m of gray dolomite layers. Upper units in the Chichakloo area contain yellow sandy dolomite with a thickness of 50 m. Similar to other regions in the Zanjan-Takab area, the age of basement units is Neoproterozoic–Cambrian. The basement units are covered as unconformity by Eocene marl, sandstone, and shale.

Pb–Zn mineralization can be seen in a boundary of sericitic schist in the footwall and within crystalline gray dolomite. Mineralization is observed to a great extent of the area with a length of 1300 m in fractures and faults in upper yellow

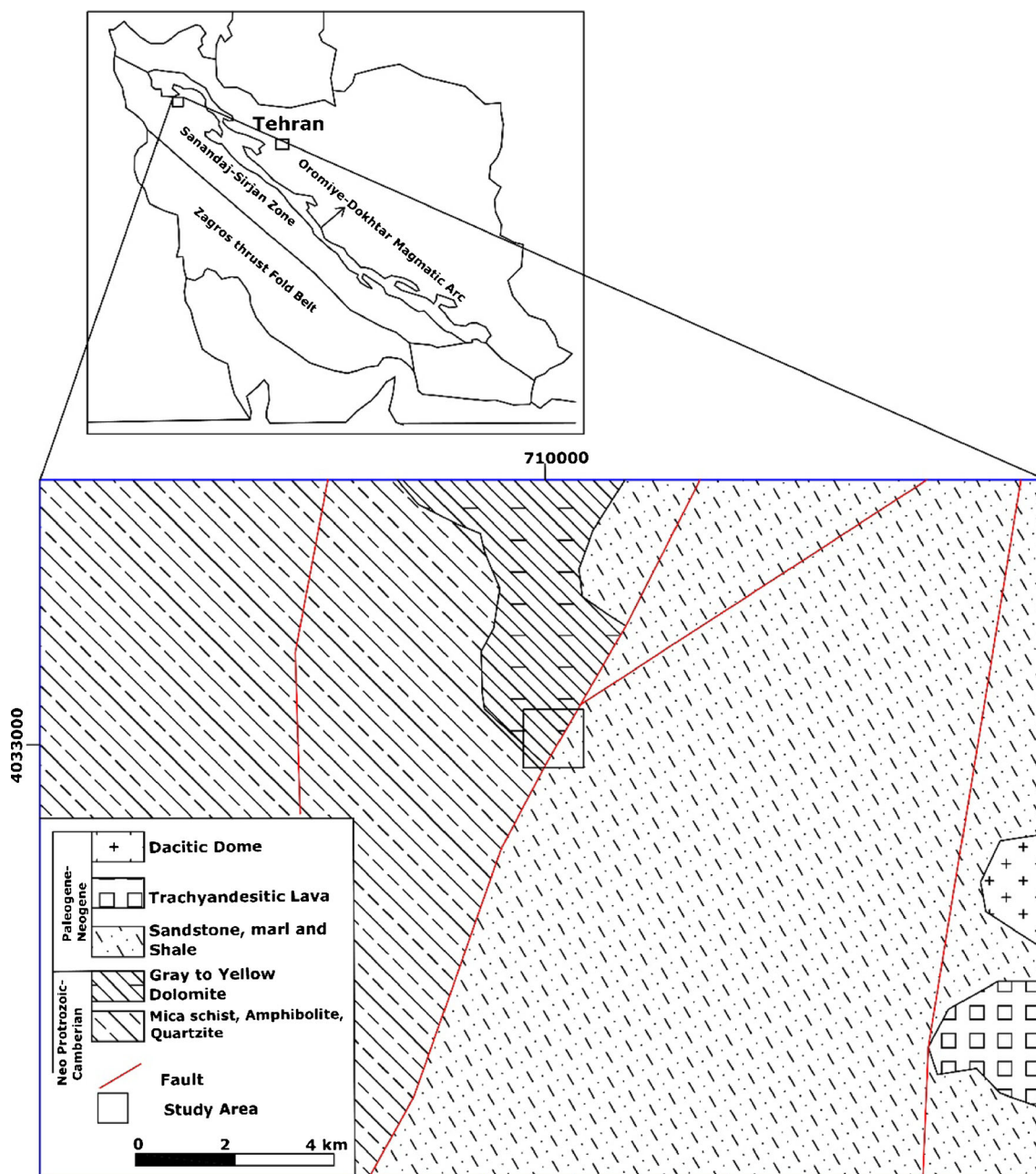


Fig. 1 a The Chichakloo area shown by a *black small rectangle* in the northwest of Iran. b A simplified geological map of the Chichakloo area; the study area is marked with a *black rectangle* in the central part (toward north) of the area

dolomite units. Pb–Zn mineralization has occurred in two types at the Chichakloo area (Karam-Soltani 1997):

- 1) Stratiform mineralization in the form of breccia in crystalline gray dolomite with thickness of about 10–12 m occurred in the border of footwall schist units. This unit is considered as the main host rock of the Pb–Zn ore deposit in the study area, and geophysical and geochemical studies were conducted in this unit (Fig. 2). The ore breccia contains the fragments of gray dolomite and various sulfides such as pyrite, sphalerite, and galena. In addition to breccia

- 2) Vein mineralization with the width of 1–2 m consists of quartz, barite, calcite, galena and also sphalerite, pyrite, and chalcopyrite that has been formed by movement of ore-mineralizing fluids into normal faults in northeast–southwest faults in the upper yellow dolomite. These veins do not form an economic deposit in the study area.

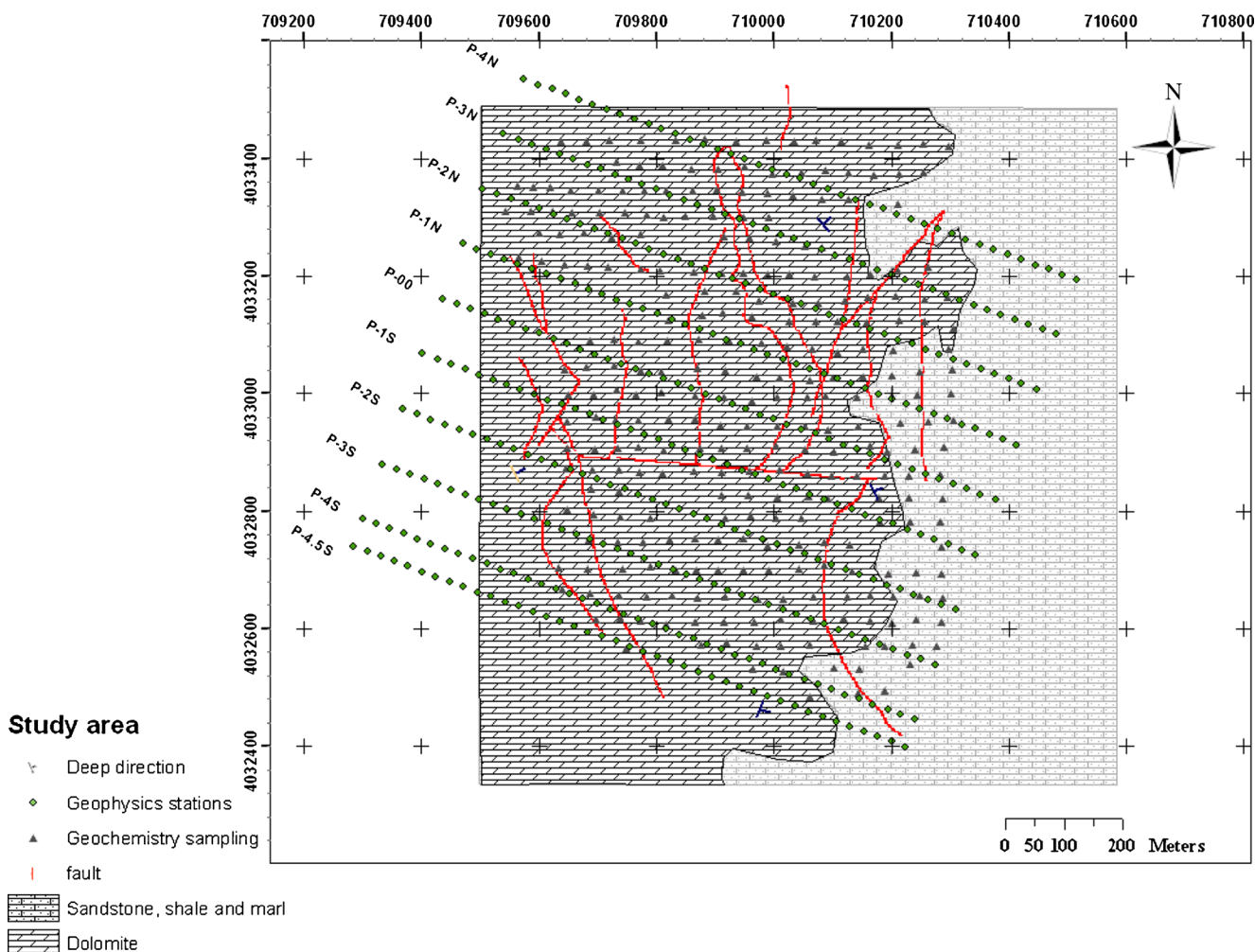


Fig. 2 Geological map of the study area showing the parallel geophysical exploration survey lines P-4n to P-4.5S aligned in the northwest–southeast direction and also the regular geochemical sampling survey grid with the nodes marked by crosses where geochemical samples are taken from

The origin of the mineralization in Chichakloo deposit is still under debate; however, the origin of Chichakloo deposit is quite similar to that of Angouran deposit in the Takab-Zanjan area due to its similarities in host rocks, structure, texture, and mineralogy (Karam-Soltani, 1997). Mineralization in Pb–Zn Angouran deposit has occurred between micaschist units in the footwall and also the main host is marble units that are of Neoproterozoic–Cambrian age. Although the mineralization type in Angouran deposit is also under debate, a recent study of Gilg et al. (2005) shows that the Angouran deposit is a new type of low-temperature mineralization in a carbonate host that differs with Mississippi Valley-type (MVT) and sedimentary exhalative mineralization. Based on the study by Leach et al. (2005), the tectonostratigraphic setting of MVT deposits is a platform carbonate sequence at flanks of basins or foreland thrust belts. The host rock of mineralization is mainly dolostone and limestone. The ore body morphology is highly variable, commonly strata bound, pipes, or tabular zones and locally stratiform.

The ore fluids are mostly low-temperature (90–150 °C) connate bittern brines or evaporate dissolution brines. Timing of mineralization is epigenetic, tens to hundreds of millions of years after host rock deposition. These deposits are not associated with igneous activity.

Geophysical investigation

Geophysical surveys using resistivity and IP methods were carried out to assess the extents of Pb–Zn mineralization in the area. The dipole–dipole electrode configuration with an electrode separation of 25 m was employed along 10 parallel lines with a distance of 100 m from each other on the dolomite unit. Inverse modeling of the resistivity and IP data was made using RES2DINV software package developed by Loke (2001).

An example of the inverse modeling results of the resistivity and IP data for the P-4.5S line (see Fig. 2) is shown in Fig. 3. The modeling results for this profile indicate the

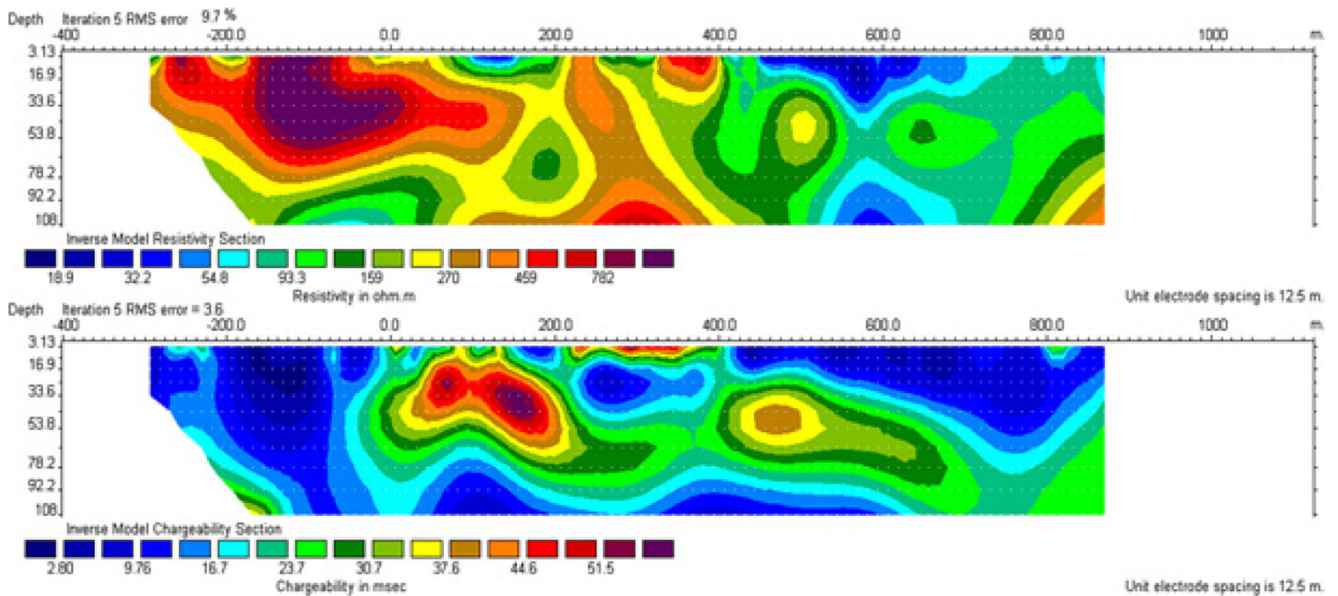


Fig. 3 2D inverse model resistivity and IP sections for line P-4.5S

presence of an anomaly with a chargeability of greater than 35 ms and a lateral extent from 0 to 225 m along the profile and a depth extent of 10 to 60 m. The resistivity of this anomaly is varying, but at a lateral extent of 125 to 225 m along the profile, it is reduced to 200 Ω m. The resistivity variations of the anomaly can imply varying mineralization texture of the anomaly, which is located in the dolomite unit as the host rock. Another anomaly with a chargeability of around 30 ms can be observed at a lateral extent of 400 to 600 m along the profile and a depth extent of 30 to 70 m. The resistivity of this anomaly is generally low but relatively varying since shale, sandstone, and clay accompany the anomaly.

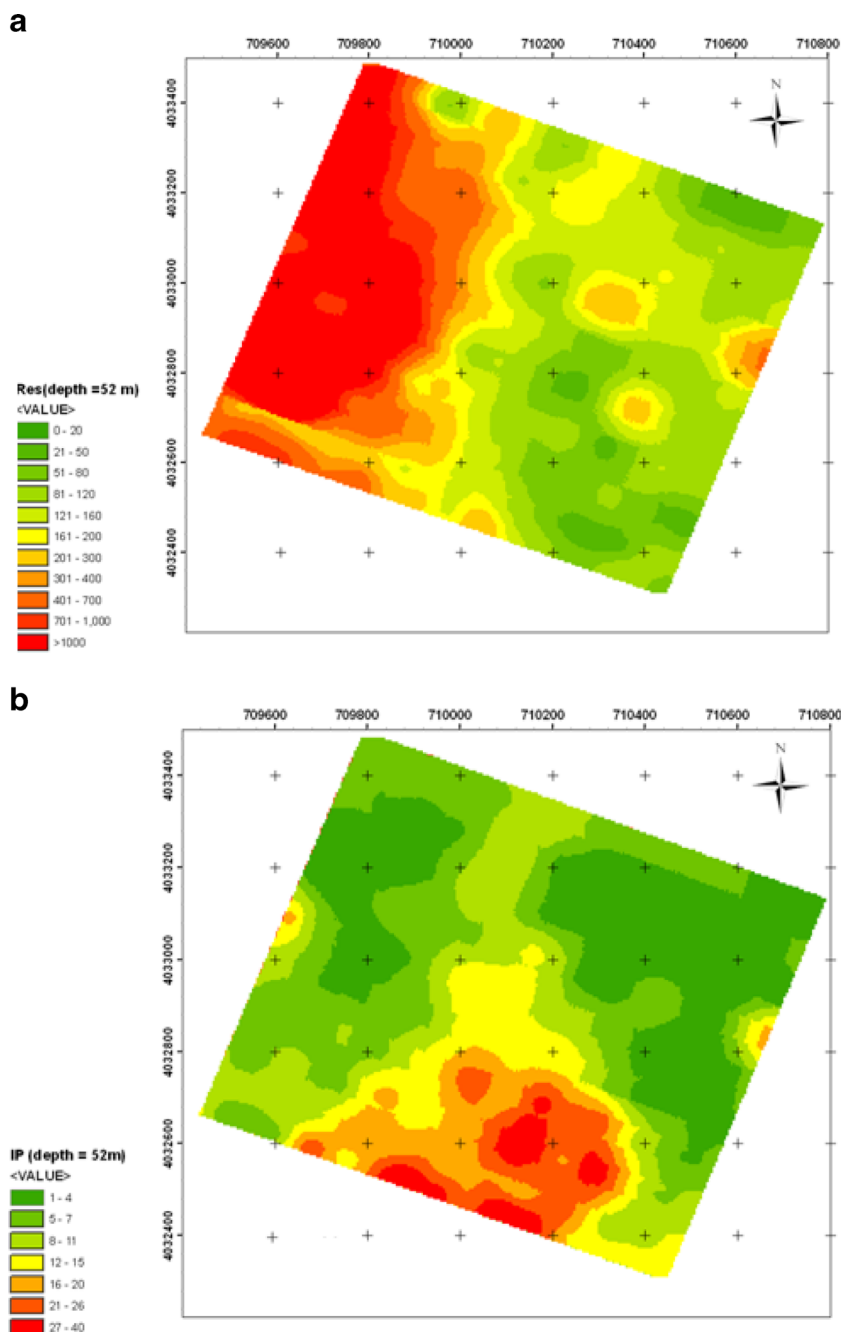
To generate resistivity and IP maps in a GIS environment, the numerical results obtained from the inverse modeling of resistivity and IP data along the 10 profiles were extracted. Based on the inverse modeling work, we obtained the resistivity and IP horizontal maps in each of 10 depth levels of 9, 16, 24, 32, 41, 52, 63, 75, 85, and 105 m. Thus, 20 resistivity and IP maps related to 10 depth levels were generated in a GIS environment. The resistivity and IP maps for the depth of 52 m are shown in Fig. 4a, b, respectively. Two different and distinct resistivity zones can be easily distinguished in Fig. 4a. One of the two zones, having a resistivity of greater than 700 Ω m, is located in the west part of the map and is embedded in the dolomite unit while the other zone, having a resistivity of less than 150 Ω m, is located in the east part of the map and is embedded in the marl, sandstone, and shale units. A considerable note observed in the resistivity map is the low resistivity values in the southwest of the map, which can indicate the presence of mineralized zones in the southwest of the study area. In the IP exploration map for the depth of 52 m (shown in Fig. 4b), we can observe an extended IP anomaly with a

chargeability of greater than 15 ms in the south of the map. An increase in the chargeability of this anomaly is evident as progress in the anomaly from west to east so that chargeability in the east of the anomaly exceeds 30 ms.

Geochemical investigation

Litho-geochemical studies have been carried out in the study area. Two hundred ninety-two samples were collected and analyzed for 44 elements. The location of samples is shown in Fig. 2. After data processing, multi-element analyses were carried out using principal component analysis (PCA) for the recognition of chemical behavior of the paragenesis elements accompanying the main elements (i.e., Pb and Zn). PCA is a multivariate statistical method for geoinformation identification of geodatasets (Cheng et al. 2011). In the PCA method, correlated variables with high dimensionality are transformed into several uncorrelated principal components (PCs) based on a covariance or correlation matrix (Loughlin 1991). PCA has been frequently used for the analysis of geochemical data in order to identify the mineralization factor(s) and determine the attributes of mineralization (e.g., Cheng et al. 2006; 2011; Davis 2002; Zuo 2011; Shahi et al. 2014). The results of PCA are shown in Table 1. The first four components represent about 77.5 % of total variance. The first PC (PC1) in Table 1 can be attributed to the decomposition of syngenetic components. In PC1, the high negative amounts of the elements Ca and Mg are related to the dolomite host rock, while the high positive values of other elements are related to the marl, sandstone, and shale units since these elements are relatively high in this unit background. The high coefficients of Zn, Pb, Au, Ag, As, Cu, Mo, Sb, and Tl elements seen in the

Fig. 4 **a** IP map at a depth of 52 m. **b** Resistivity map at a depth of 52 m



second PC (PC2) indicate the paragenesis elements accompanying Pb and Zn mineralization in the study area.

In order to generate a geochemical predictor map, we calculated the geochemical mineralization probability index (GMPI) of PC2 as proposed by Yousefi et al. (2012) using the following logistic function:

$$GMPI = \frac{e^{MFS}}{1 + e^{MFS}} \quad (1)$$

where MFS is the mineralization factor scores inferred from PC2 (Table 1). As shown by Yousefi et al. (2012), GMPI enhances

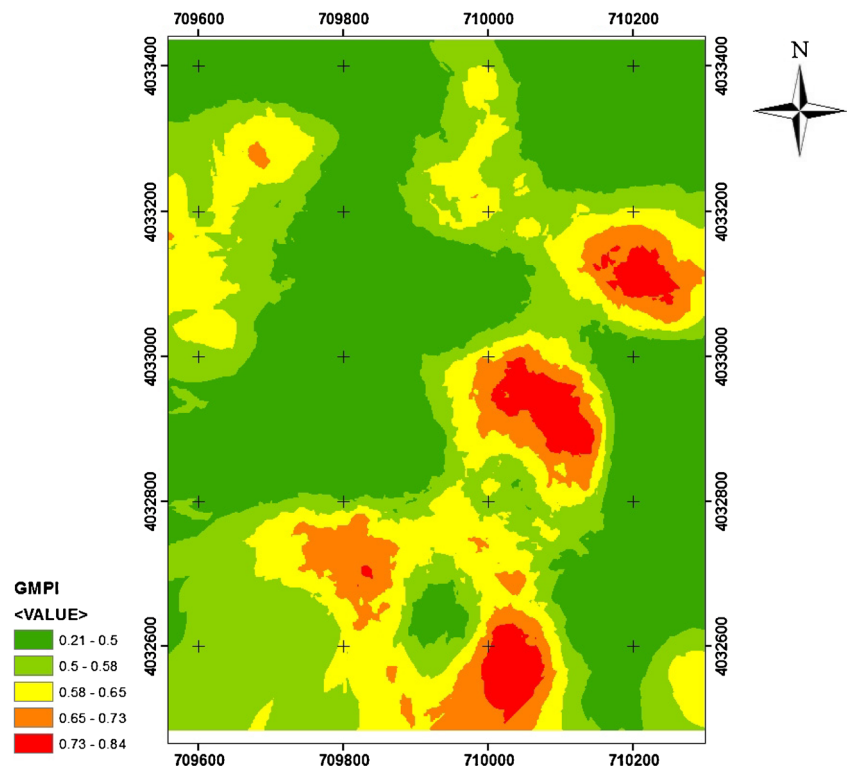
discrimination between background and anomaly and the prediction rate of a GMPI map with respect to known mineral deposit occurrences is generally higher than factor score maps. On the other hand, the values of GMPI fall in the [0, 1] range, which can be used as fuzzy weights for the integration of the geochemical predictor map with other exploration predictor maps.

The GMPI distribution map inferred from PC2 was considered as a multi-element mineralization component and is plotted in Fig. 5 to generate the geochemical predictor map. An investigation of this map indicates an extended multi-element anomaly having a strike of north–south in the east of the map.

Table 1 Rotated component matrix inferred from the PCA method. The mineralization component (PC2) and its elements were highlighted (based on the threshold of 0.6)

	Component			
	1	2	3	4
Au	-.131	.764	.018	.035
Cr	.709	.139	.039	-.322
Mn	.395	.044	.735	.222
Ni	.760	.268	.308	.083
Pb	-.364	.816	-.144	.137
Sr	.062	-.302	.729	-.205
Ba	.805	.135	.263	.029
Be	.805	-.165	.087	-.298
Ti	.968	-.147	.052	.051
Fe	.822	.348	.177	.013
Al	.928	-.142	.158	.125
Ca	-.941	-.020	.065	.123
Li	.850	.115	.128	.112
P	.922	.006	.118	.074
V	.975	-.054	.035	.026
Mg	-.931	.083	-.135	.111
K	.951	-.111	.024	.038
Na	.825	-.202	.172	.044
S	.246	.276	.019	.646
Zr	.855	-.167	.141	.171
Ag	.009	.850	-.107	-.039
As	-.224	.875	-.116	.051
Bi	.432	.496	.077	-.038
Co	.825	.225	.343	.082
Cu	.306	.733	.118	.106
Mo	.259	.619	.116	-.435
Sb	-.042	.905	-.084	.072
Zn	-.337	.730	-.166	.087
Sn	.897	.069	-.062	.056
W	.715	.161	.101	-.230
Cs	.919	-.078	.077	.043
Nb	.952	-.141	.062	.009
U	.738	.291	.064	-.022
Cd	-.564	.553	-.194	.228
Rb	.959	-.116	.064	.055
Th	.961	-.131	.122	.078
Y	.758	-.133	.298	-.089
Ce	.915	-.091	.100	.074
Tl	.419	.645	.199	-.045

Fig. 5 GMPI distribution map inferred from the mineralization component (PC2)



Materials and methods

Fuzzy logic

A fuzzy concept is a concept of which the boundaries of application can vary considerably according to context or condition. Whereas in the classical set theory an object either is or is not a member of a given set, in the fuzzy set theory, membership is a matter of degree and is defined by Zadeh (1965) as

$$\mu_A : X \rightarrow [0, 1] \tag{2}$$

where μ_A is the degree of membership of element x in the fuzzy set A for each $x \in X$. $[0, 1]$ denotes the interval of real numbers from 0 to 1, inclusive. Therefore, the value 0 is used to represent complete non-membership and the value 1 is used to represent full membership, and values in between are used to represent intermediate membership degrees. The fuzzy set, A , is usually denoted by a set of pairs:

$$A = \{(x, \mu_A(x)), x \in U\} \tag{3}$$

where U is a finite set $\{x_1, \dots, x_n\}$.

Estimation of fuzzy membership values for individual predictor maps

The fuzzification of predictor maps comprises the definition of the fuzzy membership function and the assignment of membership grades to all x in A (Robinson 2003). The

membership functions of fuzzy sets must be precisely defined in respect of function type and function parameters to assign possibilities of class occurrence to the map units. To fuzzify the resistivity and IP maps and generate a geophysical predictor map, we used the following fuzzy membership functions:

$$\mu_{RES}(X) = \begin{cases} 0 & x > 500 \\ 0.9 * \frac{(500-x)^2}{(500-150)^2} & 150 < x \leq 500 \\ 0.9 & x \leq 150 \end{cases} \tag{4}$$

$$\mu_{IP}(X) = \begin{cases} 0 & x < 10 \\ 0.9 * \frac{(x-10)^2}{(20-10)^2} & 10 \leq x < 20 \\ 0.9 & x \geq 20 \end{cases} \tag{5}$$

where μ_{RES} and μ_{IP} are the degrees of fuzzy membership corresponding to the resistivity and chargeability values of related cells in resistivity and IP maps, respectively. These functions were used based on the range of resistivity and IP variations in dolomite host rock inferred from inverted data and also the exploration target, i.e., Pb–Zn mineralization. Chargeability is regarded as favorable for Pb–Zn mineralization when it is over 20 ms. Higher values of chargeability might be influenced by the presence of pyrite (confirmed from drilling results) as a gangue mineral accompanying the Pb–Zn mineralization, and therefore, the degree of favorability of the IP map remains constant when chargeability values exceed 20 ms. The degree of favorability in the IP map decreases as the chargeability decreases and is regarded as unfavorable

when it drops to less than 10 ms. On the contrary, the degree of favorability in resistivity maps increases as the resistivity decreases and is regarded as unfavorable when it is over 500 Ω m. A resistivity less than 150 Ω m is regarded as favorable for Pb–Zn mineralization. In this separation, the presence of clay in the east of the study area has been considered and therefore, the degree of favorability of the resistivity map remains constant when resistivity drops 150 Ω m. Considering the fact that in analyzing exploration data nothing can be regarded for sure as possible, the value of 1 was restrained from predictor maps.

We have proposed a new approach in this study for the fuzzification of the GMPI map to generate the geochemical predictor map using the following fuzzy membership function:

$$GFC = \begin{cases} GMPI & GMPI > 0.5 \\ 0 & GMPI \leq 0.5 \end{cases} \quad (6)$$

where GFC is the geochemical fuzzy coefficient and GMPI is the geochemical mineralization probability index of each pixel inferred from Eq. (1). The pixels with the negative MFS in PC2 result in GMPI values of less than 0.5 which are not related to the mineralization phase. Consequently, the degree of favorability in the geochemical predictor map is regarded as unfavorable when the GMPI value drops to less than 0.5. On the contrary, the degree of favorability in the geochemical predictor map is equal to the GMPI value when the MFS is positive.

The geological map of the study area (Fig. 2) shows that the geochemical and geophysical data were collected along the dolomite and sandstone units. As discussed in “[Geological investigation](#),” the gray dolomite is considered as the main host rock of stratiform mineralization which forms an economic deposit in the study area and therefore, we assigned a high fuzzy value of 0.8 for this unit. On the other hand, a fuzzy value of 0.3 was assigned for marl, sandstone, and shale units, since the report of geological investigation reveals that this unit is much less important than the dolomite unit for economic mineralization.

Fuzzy operators

Numerous fuzzy operators have been suggested in literature (e.g., Zadeh 1973; Dubois and Prade 1985; Yager 1980; Zimmermann 1991). The final fuzzy decision depends on decision criteria including decision goals, and selected decision function should well reflect the goals of the decision. Conjunctive, disjunctive, and compensatory aggregation of criteria are widely used in fuzzy decision-making (Sousa and Kaymak 2002).

The conjunctive aggregation simultaneously satisfies all decision criteria but the second kind makes full compensation

amid the criteria. Finally, compensatory aggregation is used for handling conflicting criteria or human aggregation behavior (Sousa and Kaymak 2002). From the conjunctive aggregation operators, the fuzzy AND and product operators are widely used for the integration of exploration data when two or more evidences should simultaneously be present (Bonham-Carter 1994). From the disjunctive aggregation operators, the fuzzy OR and sum operators are widely used for the integration of exploration data when the presence of any positive evidence is sufficient for having a favorability condition (Bonham-Carter 1994).

The compensatory aggregation operators are defined by applying a combination of conjunctive aggregation and disjunctive aggregation operators. From compensatory operators, Zimmermann and Zysno (1980) defined a combination of algebraic sum and algebraic product operators as

$$E_z(\mu_1, \dots, \mu_n) = \left(\prod_{i=1}^n (\mu_i) \right)^{1-\gamma} \left(1 - \prod_{i=1}^n (1-\mu_i) \right)^\gamma \quad (7)$$

Depending on the value of γ , the result of applying this operator will always be a value between the resulting values obtained from applying the algebraic sum and algebraic product operators. This operator is extensively used in the integration of mineral exploration evidences. When $\gamma=1$, then the combination is the same as the fuzzy algebraic sum combination, and when $\gamma=0$, then the combination is the same as the fuzzy algebraic product combination.

The operators discussed above consider equal influence of each criterion in the final result. However, in some problems, some criteria may have more influences in the final result and the degree of importance of each criterion should be defined before the integration. Various fuzzy operators have been proposed for weighted aggregation (see, e.g., Kaymak and Sousa 2003). Among weighted aggregation operators, we have selected the weighted Yager t-norm fuzzy operator (Kaymak and Sousa 2003) given by the following equation for the integration of exploration data due to its efficiency and flexible compatibility between the minimum and the maximum membership functions.

$$D^w(\mu_1, \dots, \mu_n) = \max \left(0, 1 - \sqrt[s]{\sum_{i=1}^n W_i (1-\mu_i)^s} \right) \quad s > 0 \quad (8)$$

where W_i is the weight factors and are chosen between 0 and 1 and then normalized by the following mathematical expression (Kaymak 1998):

$$\sum_i^n W_i = 1 \quad (9)$$

Applying this operator on the membership functions and satisfying the condition expressed by Eq. (9), the results will always be between the lowest and highest membership functions and also will be influenced more by the criteria of

functions which possess greater weights. The weight vector in mineral potential map generation should be determined based on several important exploration factors such as the exploration target, types of exploration surveys carried out in the study area, reliability, uncertainty, and noise level in the exploration data. In addition, variations of the parameter s in this operator will make a flexible compatibility between the minimum and the maximum membership functions. Higher values of the parameter s make the tendency of the results to the minimum membership function, while lower values of the parameter s make the tendency of the results to the maximum membership function.

Results

Exploration predictor maps

Resistivity and IP modeling results for 10 different depths were fuzzified using Eqs. (4) and (5), respectively. The obtained resistivity and IP maps in different depths must be now integrated to generate the final resistivity and IP predictor maps. The main aim in this stage is to convert all depth data in three dimensions to a two-dimensional map that includes information for different depths obtained from modeling resistivity and IP data. For this purpose, we applied the operator defined by Eq. (7) with high values of γ . As a result, the anomalies, which have greater depth extensions, appear in several depths and will be enhanced, and hence, these anomalies compared to the anomalies having less depth extensions will have greater fuzzy values in the final map. The γ values equal to 0.95 for the integration of IP maps and 0.9 for the integration of resistivity maps were selected for integrations. The predictor resistivity and IP maps are shown in Fig. 6a, b, respectively.

An investigation of the IP predictor map implies the spread of an anomaly with a fuzzy value of greater than 0.5 in the south of the map. Considering the integration process of method, high fuzzy values in the IP predictor map indicate high chargeability anomalies that have relatively extensive depth spreads. This IP anomaly meets profiles P-2S, P-3S, P-4s, and P-4.5S (Fig. 2). The increasing trend of the anomaly favorability is from west to east quite evident. In the resistivity predictor map shown in Fig. 6b, the high fuzzy values are seen in the east of the study area.

For the integration of resistivity and IP maps and obtaining the geophysical predictor map, we applied the weighted fuzzy operator given by Eq. (8) using several values of s . To apply the weight vector, the relative importance of resistivity and IP maps, $W=(W_{IB}W_{Res})$, should be first defined. In exploration of sulfide deposits, the importance of the IP method is generally greater than resistivity data as there is more likely to have disseminated mineralization in the zones with high

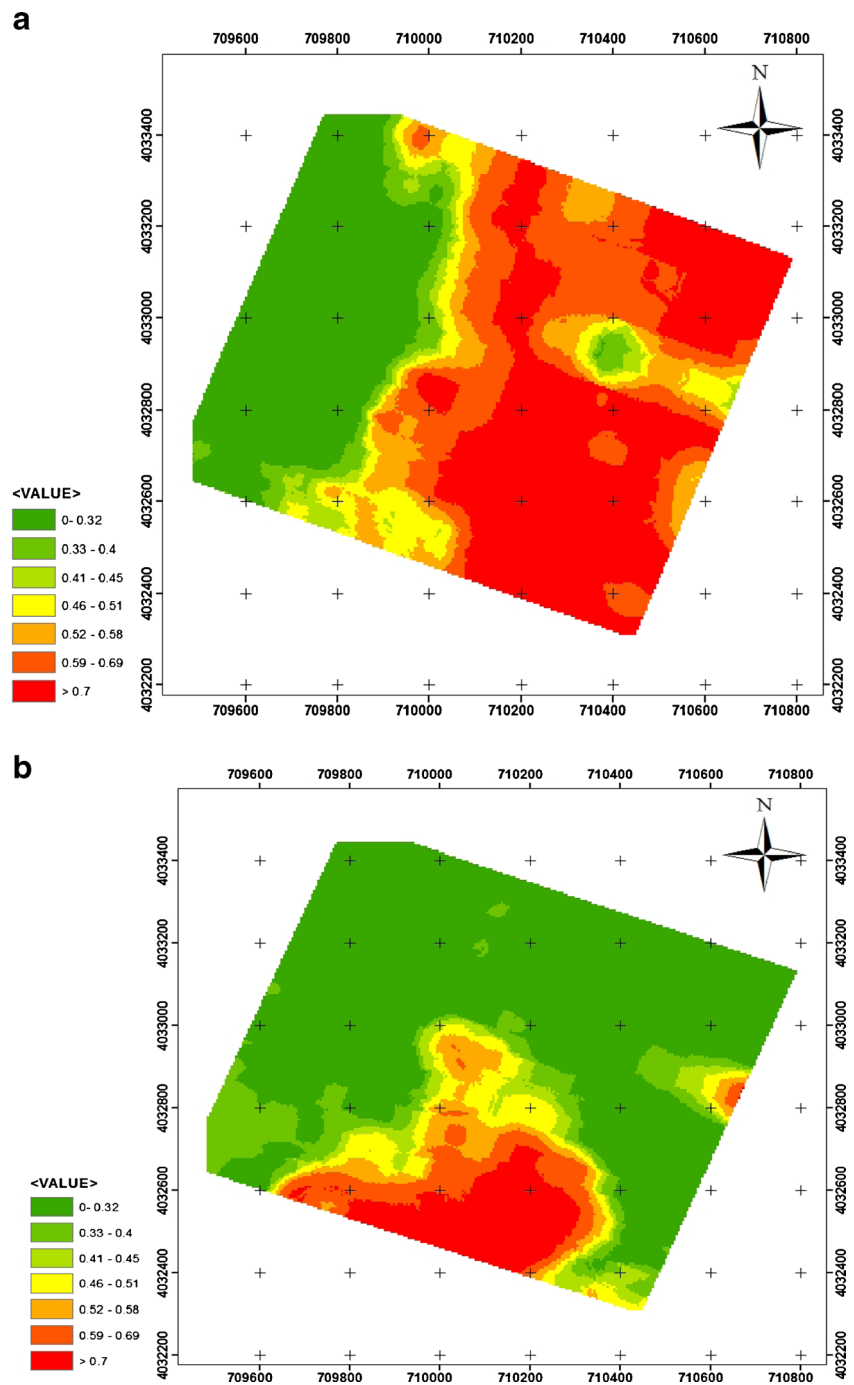
chargeability and resistivity. However the zones, which have low chargeability and resistivity are not important in terms of sulfide deposits in the area as low resistivity values in some area are irrelevant to metallic mineralization and are due to the presence of clay in the subsurface. Therefore, a value of 0.7 for weight of the IP map and consequently a value equal to 0.3 for the resistivity map were selected and the geophysical predictor map was then generated. Applying the weighted fuzzy operator given by Eq. (8) with large values of s causes a reduction in favorability of geophysical anomalies; on the other hand, small values of s in the integration of IP and resistivity data cause to have partial false anomalies. Therefore, it appears that values about $s=3$ to $s=8$ present the favorability of geophysical anomalies in the best manner. After investigating the results of the operators in the integration of resistivity and IP maps, the parameter s was selected to be 5 for the integration of resistivity and IP predictor maps. The geophysical predictor map is shown in Fig. 7. As can be seen from this map, a geophysical anomaly with fuzzy values of greater than 0.5 is evident in the south of the study area. The increasing trend of fuzzy values of this anomaly appears to be from west toward east, so that the fuzzy value in the eastern part of this anomaly exceeds 0.7.

To generate the geochemical predictor map, we used Eq. (6) to plot the GFC map. The generated geochemical predictor map is shown in Fig. 8. An investigation of this map indicates the spread of the geochemical anomaly in eastern parts of the map that has a north–south strike and is located in the dolomite unit. In some parts, the fuzzy value of this anomaly increases to 0.7. Finally, the geological predictor map was generated by assigning the fuzzy values of 0.8 for the dolomite unit and 0.3 for the marl, sandstone, and shale units.

Generation of the mineral potential map

Investigating and comparing the results of geophysical, geochemical, and geological predictor maps, we can observe a considerable overlapping between geophysical and geochemical anomalies in the dolomite unit in the south of the study area. However, for quantitative interpretation and presentation of the mineral potential map, in this stage, we have integrated geophysical, geochemical, and geological predictor maps using the weighted fuzzy operators given by Eq. (8). The weight vector was selected based on specialists' opinions. Majority of specialists gave more importance to geophysical (particularly IP) anomalies rather than geochemical anomalies due to their efficiency in Pb–Zn sulfide mineralization exploration. Moreover, geophysical maps can better estimate the extension of the anomalies which are very important in selecting drilling points. On the other hand, geochemical maps are influenced by a considerable number of censored data. Therefore, the greatest weight was selected for the

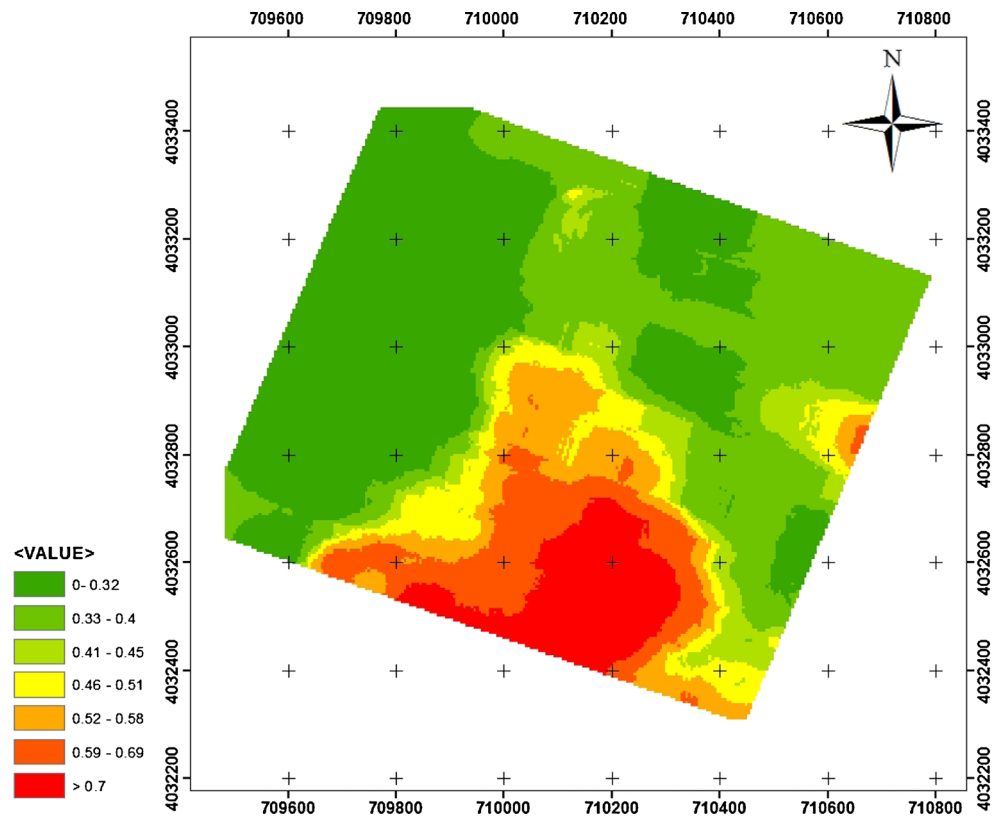
Fig. 6 **a** Resistivity predictor map obtained as a result of applying the operator given by Eq. (7) with $\gamma=0.9$. **b** IP predictor map obtained as a result of applying the operator given by Eq. (7) with $\gamma=0.95$



geophysical predictor map. The lowest weight was finally considered for the geology map. The geology map was used in order to emphasize geochemical and geophysical anomalies coinciding with the dolomite host. Since a low fuzzy favorability of 0.3 was selected for the sandstone host, therefore, integration of the geology map with a lower weight still can separate the anomalies coinciding with the dolomite host, but a greater weight for the geology map can overestimate exploration anomalies and cause misleading results for selecting the best drilling point. Therefore, the weight

vector for the final exploration map, symbolized by $W = (W_{\text{geophysical map}}, W_{\text{geochemical map}}, W_{\text{geology map}})$, was selected to be $W = (0.40, 0.35, 0.25)$. We have used values of 1, 2, 5, and 10 for parameter s in Eq. (8). The results are plotted in Fig. 9. An investigation of Fig. 9 indicates a fuzzy favorability of greater than 0.4 in the east of the study area with a north–south trend. An important and highlighted presence of an anomaly with a fuzzy favorability of more than 0.7 can be observed in all maps shown in Fig. 9, which indicates a considerable overlapping of geophysical and geochemical anomalies in

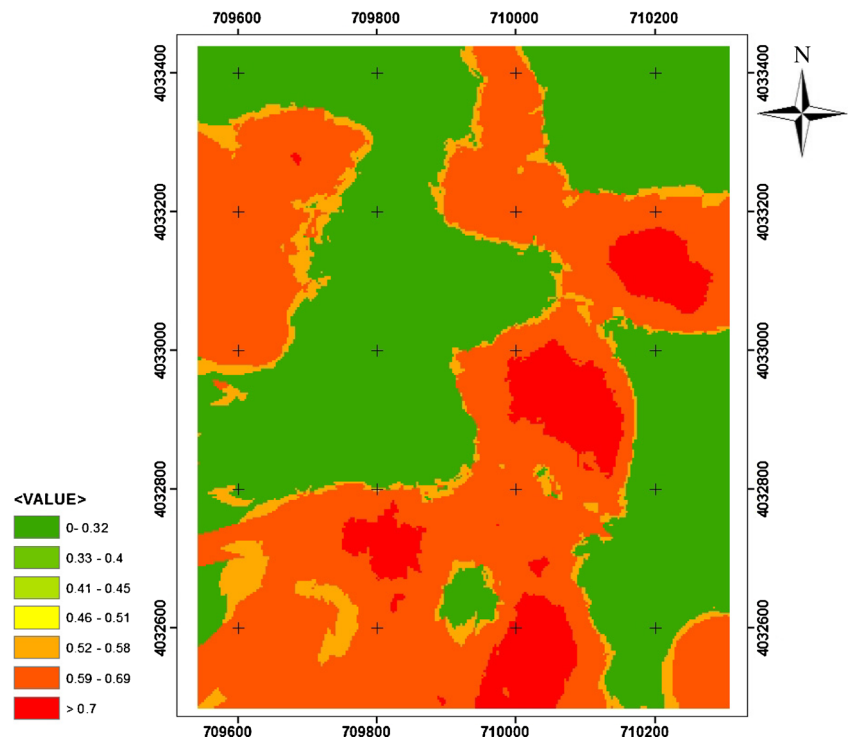
Fig. 7 Geophysical predictor map obtained as a result of applying the operator given by Eq. (8) with $s=5$



the dolomite unit. Comparing between maps in Fig. 9, we observed an overestimation of the fuzzy favorability of anomalies in Fig. 9a, b compared with maps that were produced before

integration. These maps were produced by applying $s=1$ and $s=2$. Since the final purpose of this study is to suggest drilling points, maps numbered 9c and 9d (obtained by applying $s=5$

Fig. 8 GFC map (geochemical predictor map) inferred from the mineralization component (PC2)



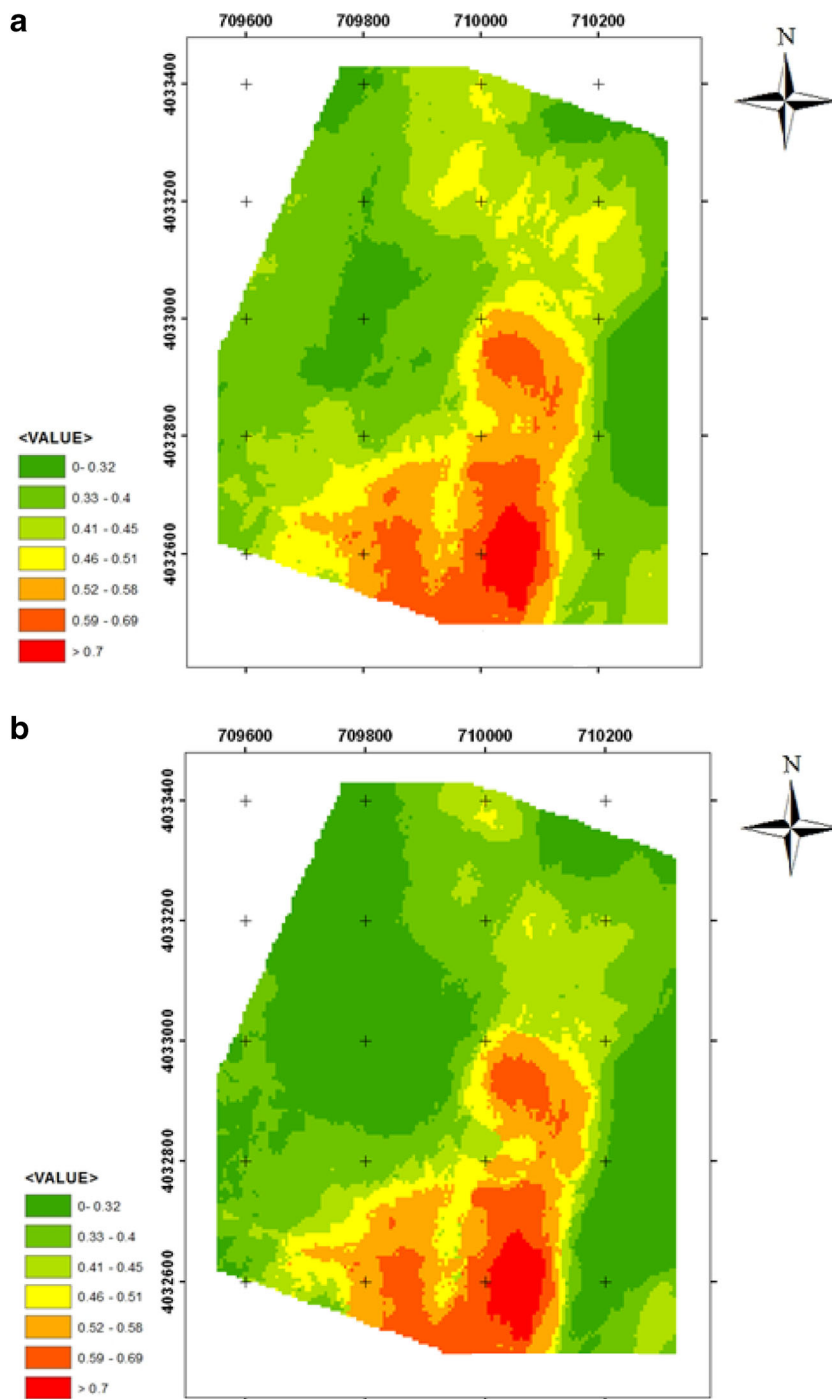


Fig. 9 Mineral potential map using the operator given by Eq. (8) with **a** $s=1$, **b** $s=2$, **c** $s=5$, and **d** $s=10$

and $s=10$, respectively) that present a more conservative estimation of anomalies were taken into account. An investigation of these maps indicates a fuzzy favorability of greater than 0.4 in the east of the study area with a north–south trend. In the south of the study area, we can see a fuzzy favorability of greater than 0.6, and thus, it is considered as the most suitable part of the area for existence of mineralized zones and drilling exploration boreholes.

Discussion and conclusions

In this study, mineral potential mapping was carried out by the integration of the fuzzified geophysical, geochemical, and geological predictor maps using the weighted fuzzy operators in the GIS environment. The weighted fuzzy operator, suggested in this study, aimed to take the importance of each predictor map into account in the production of the mineral

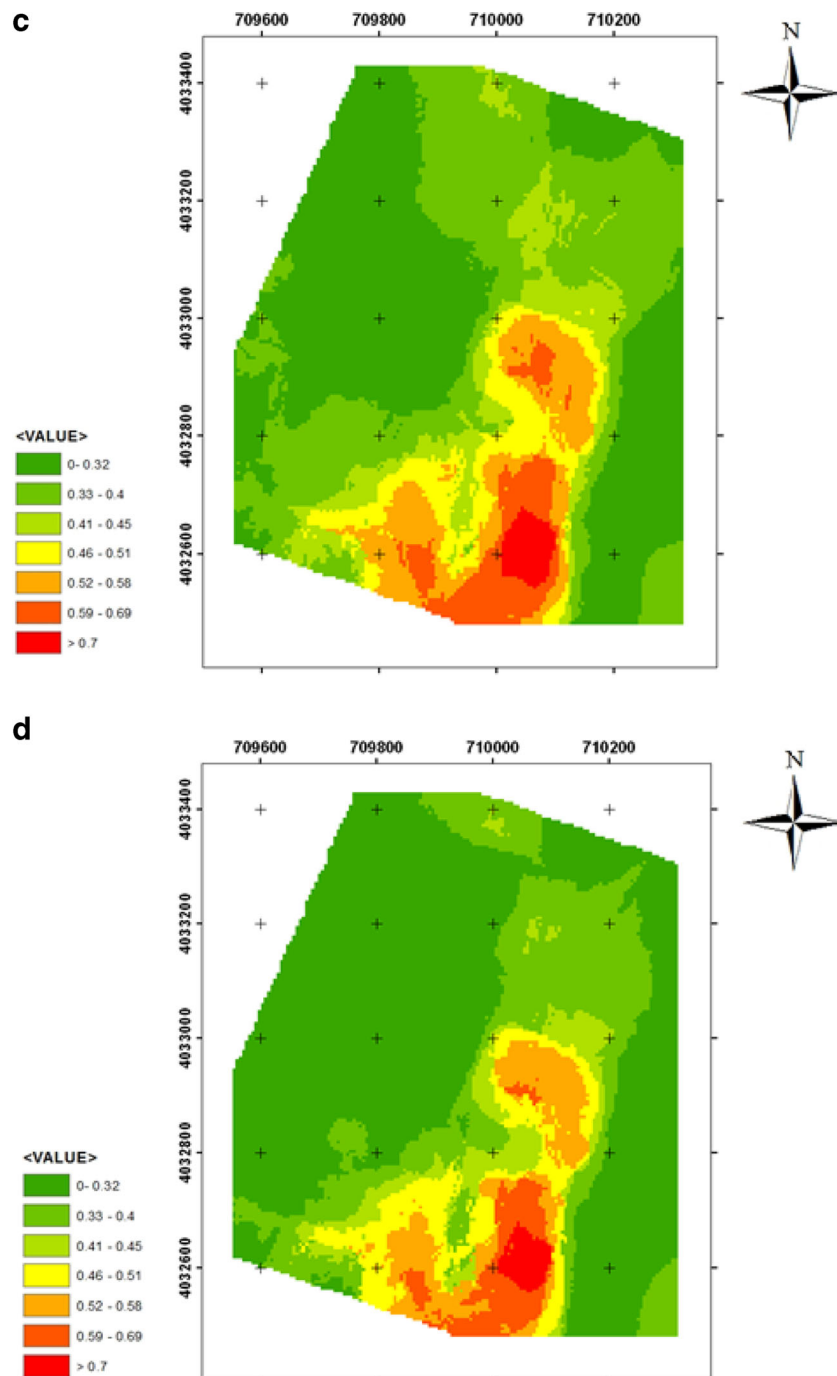


Fig. 9 continued.

potential map. Assigning the weight of each predictor map in the mineral potential mapping is not a new idea; however, our approach is slightly different from the previous studies. In the previous studies (e.g., Lisitsin et al. 2013; González-Álvarez et al. 2010; Porwal et al. 2003b), the weight of each predictor map was considered during the fuzzy membership value assignment, while in this study, the weight of predictor maps was assigned after predictor map fuzzification. In fact, the weighted fuzzy operators allow experts to better assign the

weight of predictor maps in the last stage by comparing the influence of each predictor map in the potential map generation. In this research work, we have selected one of the many weighted fuzzy operators proposed for weighted aggregation in various studies. This operator can be used as an efficient operator for the integration of exploration maps with different importance or weight values. Expert determination of the parameter s by the decision-maker can best reflect the goals of the decision. Small variations of the parameter s in Eq. (8) will

make a flexible compatibility between the minimum and the maximum membership functions. In addition, the results will be influenced more by the criteria of functions which possess greater weights.

The approach presented in this study, in order to convert and map 3D geophysical data to a 2D geophysical model of the study area that best reflects depth information, can play an effective role in the appropriate integration of geophysical data. In addition, this 2D geophysical map can be compared with 2D geochemical maps, and thus, geophysical anomalies can be compared with geological anomalies in order to determine mineralized zones in the study area.

Moreover, we have applied a logistic function to transform a multi-element mineralization factor score map to a GMPI map in order to generate the geochemical predictor map. As demonstrated in several studies (e.g., Yousefi et al. 2012; 2014), GMPI increases the geochemical anomaly intensity based on mineralization elements and consequently enhances the probability of success in mineral potential mapping in comparison with factor score maps. In addition, by selecting a suitable logistic function, continuous fuzzy scores can be assigned to every value in a map of spatial data. This avoids the intermediate step of classifying continuous spatial data based on arbitrarily chosen threshold values and overcomes exploration bias in data-driven and knowledge-driven approaches resulting from simplification and discretization of evidential values into some arbitrary classes (Yousefi and Carranza 2014; 2015). On the other hand, the GFC index proposed in this study enhances discrimination between background and anomaly by removing the effect of negative MFS which are not related to the mineralization phase. The proposed GFC can be used for effective weighting and fuzzification of geochemical data to generate a reliable geochemical predictor map for integration with other predictor maps for mineral potential mapping.

A drilling borehole in the south of the area to this date shows the existence of Pb and Zn minerals in depths of 40 to 70 m that proves the validity of the study results. The results of the suggested drilling points can be considered as evidence in the next steps for optimizing future exploration maps based on data-driven methods relying on existing proofs in this region.

Acknowledgments Financial assistance provided by Shahrood University of Technology, Iran, is greatly appreciated. The authors also need to thank Karim Karam-Soltani and Amir Emam-Jomeh for their suggestions and supply of information to this research work. The advice and assistance of Mahyar Yousefi and Ramin Hendi are gratefully acknowledged. We thank the reviewers for their constructive comments that helped us improve this paper.

References

- Alavi M (1994) Tectonics of the Zagros orogenic belt of Iran: new data and interpretation. *Tectonophysics* 229:211–238
- An P, Moon WM, Rencz AN (1991) Application of fuzzy theory for integration of geological, geophysical and remotely sensed data. *Can J Explor Geophys* 27(1):1–11
- An P, Moon WM, Bonham-Carter GF (1994a) An object-oriented knowledge representation structure for exploration data integration. *Nonrenewable Resour* 3:132–145
- An P, Moon WM, Bonham-Carter GF (1994b) Uncertainty management in integration of exploration data using the belief function. *Nonrenewable Resour* 3:60–71
- Agterberg FP (1992) Combining indicator patterns in weights of evidence modeling for resource evaluation. *Nonrenew Resour* 1(1):35–50
- Agterberg FP (2011) A modified weights-of-evidence method for regional mineral resource estimation. *Nat Resour Res* 20:95–101
- Bonham-Carter GF (1994) *Geographic information systems for geoscientists: modelling with GIS*. Pergamon Press, New York, 398 p
- Bonham-Carter GF, Agterberg FP, Wright DF (1988) Integration of geological datasets for gold exploration in Nova Scotia. *Photogramm Eng Remote Sens* 54(11):1585–1592
- Brown WM, Gedeon TD, Groves DI, Barnes RG (2000) Artificial neural networks: a new method for mineral prospectivity mapping. *Aust J Earth Sci* 47(4):757–770
- Carranza EJM, Hale M, Mangaoang JC (1999) Application of mineral exploration models and GIS to generate mineral potential maps as input for optimum land-use planning in the Philippines. *Nat Resour Res* 8(2):165–173
- Carranza EJM, Hale M (2002) Wildcat mapping of gold potential, Baguio district, Philippines. *Trans Inst Min Metall* 111:100–105
- Carranza EJM (2004) Weights-of-evidence modelling of mineral potential: a case study using small number of prospects, Abra, Philippines. *Nat Resour Res* 13:173–187
- Carranza EJM, Woldai T, Chikambwe EM (2005) Application of data-driven evidential belief functions to prospectivity mapping for aquamarine-bearing pegmatites, Lundazi district, Zambia. *Nat Resour Res* 14:47–63
- Carranza EJM, Van Ruitenbeek FJA, Hecker C, Van der Meijde M, Van der Meer FD (2008) Knowledge-guided data-driven evidential belief modeling of mineral prospectivity in Cabo de Gata, SE Spain. *J Appl Earth Obs Geoinf* 10:374–387
- Carranza EJM (2010) Improved wildcat modelling of mineral prospectivity. *Resour Geol* 60:129–149
- Carranza EJM (2011) Geocomputation of mineral exploration targets. *Comput Geosci* 37:1907–1916
- Cheng Q, Agterberg FP (1999) Fuzzy weights of evidence and its application in mineral potential mapping. *Nat Resour Res* 8:27–35
- Cheng Q, Jing L, Panahi A (2006) Principal component analysis with optimum order sample correlation coefficient for image enhancement. *Int J Remote Sens* 27(16):3387–3401
- Cheng Q, Bonham-Carter G, Wang W, Zhang S, Li W, Xia Q (2011) A spatially weighted principal component analysis for multi-element geochemical data for mapping locations of felsic intrusions in the Gejiu mineral district of Yunnan, China. *Comput Geosci* 37:662–669
- Chung CF, Agterberg FP (1980) Regression models for estimating mineral resources from geological map data. *Math Geology* 12(5):473–488
- Davis JC (2002) *Statistics and data analysis in geology*, 3rd edn. Wiley, New York, 550 pp
- Dubois D, Prade H (1985) A review of fuzzy set aggregation connectives. *Inf Sci* 36:85–121
- Eddy, B. G., Bonham-Carter, G. F., Jefferson, C. W., 1995. Mineral resource assessment of the Parry Islands, high Arctic, Canada: a GIS-

- based fuzzy logic model. In: Proc. Can. Conf. on GIS, CD ROM Session C3, Can. Ins. Geomatics, Ottawa, Canada, Paper 4.
- Fallon M, Porwal A, Guj P (2010) Prospectivity analysis of the Plutonic Marymia Greenstone Belt, Western Australia. *Ore Geol Rev* 38:208–218
- Ford A, Blenkinsop TG (2008) Combining fractal analysis of mineral deposit clustering with weights of evidence to evaluate patterns of mineralization: application to copper deposits of the Mount Isa Inlier, NW Queensland. *Australia Ore Geol Rev* 33:435–450
- Ford A, Hart CJ (2013) Mineral potential mapping in frontier regions: a Mongolian case study. *Ore Geol Rev* 51:15–26
- Fung CC, Iyer V, Brown W, Wong KW (2005) Comparing the performance of different neural networks architectures for the prediction of mineral prospectivity. In: Proceedings of the Fourth International Conference on Machine Learning and Cybernetics. Guangzhou, pp 394–398
- Gilg HA, Boni M, Balassone G, Allen CR, Banks D, Moore F (2005) Marble-hosted sulfide ores in the Anguran Zn-(Pb-Ag) deposit, NW Iran: interaction of sedimentary brines with a metamorphic core complex. *Mineral Deposita* 41:1–16
- González-Álvarez I, Porwal A, Beresford SW, McCuaig TC, Maier WD (2010) Hydrothermal Ni prospectivity analysis of Tasmania. *Australia Ore Geol Rev* 38:168–183
- Hamdi B (1995) Precambrian–Cambrian deposits in Iran. In: Hushmandzadeh A (ed) Treatise of the geology of Iran, vol 20. Geological Survey of Iran, Tehran, 535p
- Harris JR, Wilkinson L, Heather K, Fumerton S, Bernier MA, Ayer J, Dahn R (2001) Application of GIS processing techniques for producing mineral prospectivity maps—a case study: mesothermal Au in the Swayze Greenstone Belt, Ontario. *Canada Nat Resour Res* 10: 91–124
- Harris DP, Zurcher L, Stanley M, Marlow J, Pan G (2003) A comparative analysis of favourability mappings by weights of evidence, probabilistic neural networks, discriminant analysis, and logistic regression. *Nat Resour Res* 12:241–255
- Harris JR, Sanborn-Barrie M, Panagapko DA, Skulski T, Parker JR (2006) Gold prospectivity maps of the Red Lake greenstone belt: application of GIS technology. *Can J Earth Sci* 43:865–893
- Joly A, Porwal A, McCuaig TC (2012) Exploration targeting for orogenic gold deposits in the Granites–Tanami Orogen: mineral system analysis, targeting model and prospectivity analysis. *Ore Geol Rev* 48: 349–383
- Karam-Soltani K (1997) Report on exploration operations for lead and zinc in Chichakloo area, Iranian Ministry of Industries and Mines (in Persian)
- Kaymak U (1998) Fuzzy decision making with control applications. PhD Thesis, Delft University of Technology, Delft, The Netherlands
- Kaymak U., Sousa, J.M., 2003. Weighted constraint aggregation in fuzzy optimisation. Kluwer Academic Publishers, Netherlands
- Leach, D.L., Sangster, D.F., Kelley, K.D., Large, R.R., Garven, G., Allen, C.R., Gutzmer, J., Walters, S. (2005) Sediment-hosted lead-zinc deposits: a global perspective. *Economic Geology*, 100th Anniversary Volume, Lancaster, PA, p561–607
- Lisitsin VA, González-Álvarez I, Porwal A (2013) Regional prospectivity analysis for hydrothermal-remobilised nickel mineral systems in western Victoria. *Australia Ore Geol Rev* 52:100–112
- Loke, M. H., 2001. Tutorial: 2-D and 3-D electrical imaging surveys. Course Notes for USGS Workshop “2-D and 3-D Inversion and Modeling of Surface and Borehole Resistivity Data”, Storrs, CT
- Loughlin WP (1991) Principal component analysis for alteration mapping. *Photogramm Eng Remote Sens* 57(9):1163–1169
- Lusty PAJ, Scheib C, Gunn AG, Walker ASD (2012) Reconnaissance-scale prospectivity analysis for gold mineralisation in the Southern Uplands-Down-Longford Terrane, Northern Ireland. *Nat Resour Res* 21:359–382
- McCammom RB (1973) Nonlinear regression for dependent variables. *Math Geol* 5:365–375
- Moon WM (1990) Integration of geophysical and geological data using evidential belief function. *IEEE Trans Geosci Remote Sens* 28:711–720
- Moon WM (1993) On mathematical representation and integration of multiple geoscience data sets. *Can J Remote Sens* 19:663–667
- Nykanen V (2008) Radial basis functional link nets used as a prospectivity mapping tool for orogenic gold deposits within the Central Lapland Greenstone Belt, Northern Fennoscandian Shield. *Nat Resour Res* 17:29–48
- Porwal A, Das RD, Chaudhary B, Gonzalez-Alvarez I, Kreuzer O (2014) Fuzzy inference systems for prospectivity modeling of mineral systems and a case-study for prospectivity mapping of surficial uranium in Yeelirrie area. *Ore Geol. Rev, Western Australia*
- Porwal A, Kreuzer OP (2010) Introduction to the special issue: mineral prospectivity analysis and quantitative resource estimation. *Ore Geol Rev* 38(3):121–127
- Porwal A, Carranza EJM, Hale M (2006) Bayesian network classifiers for mineral potential mapping. *Comput Geosci* 32(1):1–16
- Porwal A, Carranza EJM, Hale M (2004) A hybrid neuro-fuzzy model for mineral potential mapping. *Math Geol* 36:803–826
- Porwal A, Carranza EJM, Hale M (2003a) Artificial neural networks for mineral potential mapping. *Nat Resour Res* 12:155–171
- Porwal A, Carranza EJM, Hale M (2003b) Knowledge-driven and data-driven fuzzy models for predictive mineral potential mapping. *Nat Resour Res* 12(1):1–25
- Robinson VB (2003) A perspective on the fundamentals of fuzzy sets and their use in geographic information systems transactions in GIS 73–30
- Shahi H, Ghavami R, Kamkar Rouhani K, Asadi-Haroni H (2014) Identification of mineralization features and deep geochemical anomalies using a new FT-PCA approach. *J Geopersia* 4(2):101–110
- Sinclair AJ, Woodsworth GJ (1970) Multiple regression as a method of estimating exploration potential in an area near Terrace, B.C. *Econ Geol* 65(8):998–1003
- Singer DA, Kouda R (1996) Application of a feedforward neural network in the search for Kuroko deposits in the Hokuroku District, Japan. *Math Geol* 28(8):1017–1023
- Singer DA, Kouda R (1997) Classification of mineral deposits into types using mineralogy with a probabilistic neural network. *Nonrenewable Resour* 6(1):27–32
- Sousa, J.M., Kaymak, U., 2002. Fuzzy decision making in modeling and control. World Scientific
- Stockli DF, Hassanzadeh J, Stockli LD, Axen GJ, Walker JD, Dewane TJ (2004) Structural and geochronological evidence for Oligo-Miocene intra-arc low-angle detachment faulting in the Takab–Zanjan area, NW Iran. *Abstr Programs Geol Soc Am* 36(5):319
- Tangestani MH, Moore F (2001) Porphyry copper potential mapping using the weights-of-evidence model in a GIS, northern Shahr-e-Babak, Iran. *Aust J Earth Sci* 48:695–701
- Tangestani MH, Moore F (2003) Mapping porphyry copper potential with a fuzzy model, northern Shahr-e-Babak, Iran. *Aust J Earth Sci* 50(3):311–317
- Yager RR (1980) On a general class of fuzzy connectives. *Fuzzy Sets Syst* 4:235–242
- Yousefi M, Kamkar-Rouhani A, Carranza EJM (2012) Geochemical mineralization probability index (GMPI): a new approach to generate enhanced stream sediment geochemical evidential map for increasing probability of success in mineral potential mapping. *J Geochem Explor* 115:24–35
- Kamkar-Rouhani M, Yousefi M, Carranza EJ (2013) Weighted drainage catchment basin mapping of stream sediment geochemical anomalies for mineral potential mapping. *J Geochem Explor* 128:88–96

- Yousefi M, Kamkar-Rouhani A, Carranza EJM (2014) Application of staged factor analysis and logistic function to create a fuzzy stream sediment geochemical evidence layer for mineral prospectivity mapping. *Geochem: Explor Environ, Anal* 14(1):45–58
- Yousefi, M., Carranza, E. J. M., 2014. Data-driven index overlay and Boolean logic mineral prospectivity modeling in greenfields exploration. *Nat. Resour. Res.* doi: [10.1007/s11053-014-9261-9](https://doi.org/10.1007/s11053-014-9261-9)
- Yousefi M, Carranza EJM (2015) Fuzzification of continuous-value spatial evidence for mineral prospectivity mapping. *Comput Geosci* 74: 97–109
- Zadeh LA (1965) Fuzzy sets. *IEEE Information and Control* 8(3):338–353
- Zadeh, L. A., 1973. Outline of a new approach to the analysis of complex systems and decision processes. *IEEE Transactions on System, Man and Cybernetics*, SMC3, 28–44
- Zimmermann HJ (1991) *Fuzzy set theory and its application*, 2nd edn. Kluwer Academic Publishers, Boston
- Zimmermann HJ, Zysno P (1980) Latent connectives in human decision making. *Fuzzy Sets Syst* 4:37–51
- Zuo R (2011) Identifying geochemical anomalies associated with Cu and Pb–Zn skarn mineralization using principal component analysis and spectrum—area fractal modeling in the Gangdese Belt, Tibet (China). *J Geochem Explor* 111:13–22